4th Thermal and Fluids Engineering Conference (TFEC)
April 14–17, 2019
Las Vegas, NV, USA

TFEC-2019-28426

TURBULENCE MODELING OF BOUNDARY LAYERS SUBJECT TO VERY STRONG FAVORABLE PRESSURE GRADIENT (FPG) WITH PASSIVE SCALAR TRANSPORT

German Saltar[1*], Guillermo Araya[1]

[1]University of Puerto Rico, Mayaguez, PR 00681, USA

ABSTRACT

Turbulent boundary layers subject to severe acceleration or strong favorable pressure gradient (FPG) are of fundamental and technological importance. Scientifically, they elicit great interest from the points of view of scaling laws, the complex interaction between the outer and inner regions, and the quasi-laminarization phenomenon. Many flows of industrial and technological applications are subject to strong acceleration such as convergent ducts, turbines blades and nozzles. Our recent numerical predictions (J. Fluid Mech., vol. 775, pp. 189-200, 2015) of turbulent boundary layers subject to very strong FPG with high spatial/temporal resolution, i.e. Direct Numerical Simulation (DNS), have shown a meaningful weakening of the Reynolds shear stresses with an evident logarithmic behavior. In the present study, assessment of three different turbulence models (Shear Stress Transport, *k*-*ω* and Spalart-Allmaras, henceforth SST, *k*-*ω* and SA, respectively) in Reynolds-averaged Navier-Stokes (RANS) simulations is performed. The main objective is to evaluate the ability of popular turbulence models in capturing the characteristic features present during the quasi-laminarization phenomenon in highly accelerating turbulent boundary layers. Favorable pressure gradient is prescribed by a top converging surface (sink flow) with an approximately constant acceleration parameter of $K = 4.0 \times 10^{-6}$. Furthermore, the quasi-laminarization effect on the temperature field is also examined by solving the energy equation and assuming the temperature as a passive scalar. Validation of RANS results is carried out by means of a large DNS dataset.

KEY WORDS: RANS, DNS, passive scalar, quasi-laminarization, turbulence modeling.

1. INTRODUCTION

Turbulent boundary layers subject to very strong favorable pressure gradient (FPG) or acceleration are of great fundamental and technological importance, for instance flows in convergent ducts, turbines blades and nozzles. A particular type of FPG flow is the sink flow, i.e. flows developing between two straight convergent surfaces. A sink flow is characterized by a constant value of the acceleration parameter $K = \nu/U^2_\infty \, dU^2_\infty/dx$; where ν is the fluid kinematic viscosity, U_∞ is the freestream velocity, and x is the streamwise coordinate. Furthermore, it represents the only kind of turbulent flow with varying freestream velocity in which complete self-similarity can be achieved since both the outer and inner (or viscous) turbulent length scales grow at the same rate [1]. Jones & Launder [2] experimentally studied sink-flow

*Corresponding Author: german.saltar1@upr.edu

turbulent boundary layers for $K = 1.5$, 2.5 and 3×10^{-6}, respectively. The peak of the calculated Reynolds shear stresses $u'v'$, obtained from the measured mean velocity profiles and an integrated similarity equation, became gradually a smaller fraction of the measured wall shear stress as the acceleration parameter K was increased. In experimental and theoretical studies in sink flows at mild FPGs, i.e. at $K = 2.7$, 3.59 and 5.39×10^{-7}, Jones, Marusic & Perry [3] reported logarithmic behaviors in both streamwise and spanwise Reynolds stress profiles as predicted by the fully turbulent scaling laws of Perry, Henbest & Chong [4]. Scientifically speaking, an important phenomenon in fluid dynamics is when an initially turbulent boundary layer is subject to a very strong FPG, which may cause quasi-laminarization or "soft" relaminarization [5], in which "there may be appreciable residual turbulence". According to Narasimha & Sreenivasan [6] "reversion in such flows is primarily the result of the domination of pressure forces over nearly frozen Reynolds stresses, rather than of absorption or dissipation, although these could contribute (especially the latter, near the wall)". There is a region located upstream of the quasi-laminarization process, called "laminarescent" by Schraub & Kline [7] and Sreenivasan [8], where the flow parameters exhibit significant deviations from those of the canonical boundary layer or constant-pressure region but the flow still shows turbulent characteristics with significant values of the wall shear stress. Dixit & Ramesh [9] performed investigation in turbulent sink-flow and relaminarization boundary layers by means of hot-wire anemometry with the purpose of evaluating large scale motions. They considered acceleration parameters, K, in the range of $(0.77 - 4.52)\times10^{-6}$ and observed a systematic decrease of inclination angles of turbulent structures as the FPG increased. More recently, DNS of highly accelerated turbulent boundary layers [10] has revealed that the Reynolds shear stress, $u'v'$, monotonically decreased downstream and exhibited a logarithmic behaviour. Moreover, it has been hypothesized by Araya and Rodriguez [11] that decaying $u'v'$ in strong FPG flows was principally due to the annihilation of sweeps, while ejections were responsible for the turbulence residual.

In summary, while most of previous studies have focused on the velocity flow field of FPG flows with eventual quasi-laminarization, in the present study we are evaluating the effects of flow acceleration on the heat transfer. Furthermore, a detailed numerical analysis is carried out to assess three popular turbulence models (SST, k-ω and SA) on capturing the relaminarizing phenomenon.

2. NUMERICAL DETAILS

In this section, details of the different numerical tools employed is supplied. The principal approach is based on Reynolds-averaged Navier-Stokes (RANS) simulations together with the energy conservation equation, assuming temperature as a passive scalar. Direct simulations of the governing equations have also carried out in a prior study [10]; however, the most important aspects are highlighted here for reader convenience.

2.1 RANS Approach

Siemen's STAR-CCM+ [14] is a Computational Aided Engineering (CAE) software package for solving fluid and solid continuum mechanics problems. Its capabilities includes Computer Aided Design (CAD) import and generation, meshing operations, visualization, and data analysis. The RANS approach was modeled in a 2D domain as an incompressible flow. The segregated flow and segregated temperature solvers were used. These solvers use the SIMPLE algorithm to compute the governing equations using the finite volume method in a sequential manner. The steady state conservation of mass, linear momentum, and energy equations for incompressible flow and no external forces can be stated as:

$$\nabla \cdot \overline{\boldsymbol{v}} = 0 \tag{1}$$

$$\nabla \cdot (\rho \overline{\boldsymbol{v}} \otimes \overline{\boldsymbol{v}}) = -\nabla \cdot \bar{p}\boldsymbol{I} + \nabla \cdot (\boldsymbol{T} + \boldsymbol{T_t}) \tag{2}$$

$$\oint_A \rho T \boldsymbol{v} \cdot d\boldsymbol{a} = \oint_A \boldsymbol{J}_j \cdot d\boldsymbol{a} \tag{3}$$

where ρ is the density, $\overline{\boldsymbol{v}}$ and $\bar{p}$ are the mean velocity and pressure respectively, $\boldsymbol{I}$ the identity tensor, $\boldsymbol{T}$ the viscous stress tensor, $\boldsymbol{T_t}$ the Reynolds stress tensor, $\otimes$ denotes the Kronecker product, and $\boldsymbol{J}_j$ the diffusion flux. The eddy viscosity approach attempts to model the Reynolds stress tensor, $\boldsymbol{T_t}$, in terms of resolved mean flow quantities. The models were created using the analogy between the molecular gradient-diffusion and turbulent motion. The Boussinesq approximation is given by:

$$\boldsymbol{T_t} = 2\mu_t\boldsymbol{S} - \frac{2}{3}(\mu_t \nabla\cdot\overline{\boldsymbol{v}})\boldsymbol{I} \tag{4}$$

where $\boldsymbol{S}$ is the mean strain rate tensor and μ_t the turbulent Eddy viscosity, is used by STAR-CCM+ to model the Reynolds stress tensor. Additional transport equations given by turbulence models such as SA, *k-ω*, and SST are used to derive μ_t. SA defines μ_t as;

$$\mu_t = \rho f_{v1}\tilde{v} \tag{5}$$

where f_{v1} is a damping function and $\tilde{v}$ is the diffusivity. SA uses the following transport equation for a steady state problem to solve for $\tilde{v}$ and thus calculate μ_t:

$$\nabla\cdot(\rho\tilde{v}\overline{\boldsymbol{v}}) = \frac{1}{\sigma_{\tilde{v}}}\nabla\cdot[(\mu+\rho\tilde{v})\nabla\tilde{v}] + P_{\tilde{v}} + S_{\tilde{v}} \tag{6}$$

where $\sigma_{\tilde{v}}$ is a model coefficient, μ is the dynamic viscosity, $P_{\tilde{v}}$ is the production term, and $S_{\tilde{v}}$ is the user-specified source term. The definition for the turbulent Eddy viscosity used by the *k-ω* and SST models can be expressed as:

$$\mu_t = \rho k T \tag{7}$$

where *T* is the turbulent time scale and *k* is the turbulent kinetic energy. *T* is defined differently for each model and is given by:

$$T = \frac{\alpha^*}{\omega} \tag{8}$$

and

$$T = \min\left(\frac{\alpha^*}{\omega}, \frac{a_1}{SF_2}\right) \tag{9}$$

for SST and k-omega, respectively, where α^* and a_1 are model coefficients and F_2 is a blending function. The transport equations for turbulent kinetic energy and dissipation are:

$$\nabla\cdot(\rho k\overline{\boldsymbol{v}}) = \nabla\cdot[(\mu+\sigma_k\mu_t)\nabla k] + P_k - \rho\beta^* f_{\beta^*}(\omega k - \omega_0 k_0) + S_k \tag{10}$$
$$\nabla\cdot(\rho\omega\overline{\boldsymbol{v}}) = \nabla\cdot[(\mu+\sigma_\omega\mu_t)\nabla\omega] + P_\omega - \rho\beta f_\beta(\omega^2 - \omega_0^2) + S_\omega \tag{11}$$

where σ_k and σ_ω are model coefficients, P_ω and P_k are production terms, f_{β^*} is the free-shear modification factor, f_β is the vortex-stretching modification factor, S_ω and S_k are user-specified source terms, and ω_0 and k_0 are ambient turbulence values that counteract turbulence decay[14].

Velocity inlet and pressure outlet boundary conditions were specified at the extremities of the domain (Fig. 1). Velocity and temperature profiles from the DNS approach were prescribed at the inlet. At the bottom

boundary, a no-slip and isothermal wall condition was specified for the velocity and temperature field, respectively. A symmetry plane condition was selected for the top boundary. Using this condition, the shear stress and heat flux at the symmetry face is zero. However, the face value for temperature, pressure, and velocity is extrapolated from the adjacent cell using
reconstruction gradients.

Fig. 1 Schematic of the RANS computational domain.

Initial conditions were assumed 101kPa, 313 K, [1,0] m/s, and 10 for pressure, static temperature, streamwise velocity, and turbulent viscosity ratio, respectively.

2.2 DNS Approach

DNS is a numerical tool that resolves all turbulence length/time scales; thus, it aims to provide high spatial/temporal thermal-fluid data within a computational domain. Furthermore, turbulent boundary layers that evolve along the flow direction (i.e., spatially-developing boundary layers) pose an enormous challenge due to the need for time-dependent inflow turbulence information. Furthermore, accounting for the effects of strong flow acceleration adds significant complexity to the problem since the turbulent boundary layer becomes thinner, and a high spatial resolution is required in the near wall region. We are using of the Dynamic Multi-scale Approach [12], a method for prescribing realistic turbulent velocity in flow boundary conditions, which is based on the rescaling- recycling method proposed by Lund et al. [13]. The seminal idea of the rescaling-recycling method is to prescribe time-dependent turbulent information at the inlet plane based on the scaled flow solution downstream, from the "recycle" plane (see Fig. 2). Additionally, in our innovative approach there is no need to use empirical correlations to compute inlet parameters, as in the methodology introduced by Lund et al. [13]. In order to calculate the inlet friction velocity (u_τ) and friction temperature (θ_τ), an additional plane is involved, the so called "test" plane located between the inlet and recycle stations (Fig. 2). The computational domain consists of a ZPG region or precursor zone for inflow turbulent information generation of $20\delta_{inlet}$-length followed by a FPG region of $40\delta_{inlet}$-length, where δ_{inlet} is the measured 99% boundary layer thickness at the inlet. Favorable pressure gradient is prescribed by a top converging surface (sink flow) with an approximately constant acceleration parameter of $K = 4.0 \times 10^{-6}$. Dimensions of the composite computational domain (L_x, L_y and L_z) are $60\delta_{inlet}$, $4.3\delta_{inlet}$ and $4.3\delta_{inlet}$ along the streamwise (x), wall-normal (y) and spanwise (z) directions, respectively. The mesh configuration is $600 \times 80 \times 80$, which represents the numbers of points along x, y and z directions, respectively. The mesh resolution in wall units is $\Delta x^+ = \Delta x\, u_\tau / \nu = 15$, $\Delta y^+_{\min} = 0.2$, $\Delta y^+_{\max} = 13$ and $\Delta z^+ = 8$. The Courant-Friedrichs-Levy (CFL) parameter is fixed at 0.24 during the simulation and the time step is $\Delta t^+ = 0.19$.

3. DISCUSSION OF RESULTS

3.1 Grid Independence Test

A grid independence testing was conducted with the purpose of finding the most efficient meshing parameters for the RANS model. Three meshes were tested with equidistant node distribution in the streamwise x-direction. The distribution in the y direction was set as two-sided hyperbolic. The distance between the wall and the first off-wall point as well as resolution near the top surface were specified (see details in Table 1) allowing for a finer mesh inside the boundary layer and a coarser one far from the wall, as seen in Fig. 3. The SA turbulence model was used with Δy^+_{min} lower than one for all three cases (see Fig. 4a). All boundary layer parameters were post-processed by means of a MATLAB code. The Δy^+_{min} shows an incremental behavior in the FPG zone which is consistent with the increase of the local friction velocity due to the acceleration enforced to the flow. Convergence criteria was considered satisfied when the residuals of the governing equations exhibited a consistent and approximately constant behaviour. In Fig. 4b, the time history of transport equation residuals are depicted. It can be observed that after 15,000 iterations, all residuals have reached a significant decrease, atmost, of five orders of magnitude. The numerical transient took approximately 25,000 iterations. The streamwise development of the freestream velocity is exhibited in Fig. 5. All the velocities obtained were normalized by the inlet freestream velocity (1 m/s).

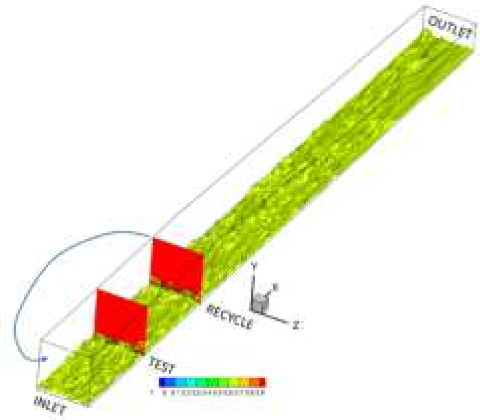

Fig. 2 Schematic of the DNS computational domain.

Table 1 Grid independence test mesh details.

	N_x	N_y	Δy_{first}	Δy_{last}
Coarse	300	50	1.48E-04	0.035
Medium	400	200	3.78E-05	0.017
Fine	600	200	3.78E-05	0.017

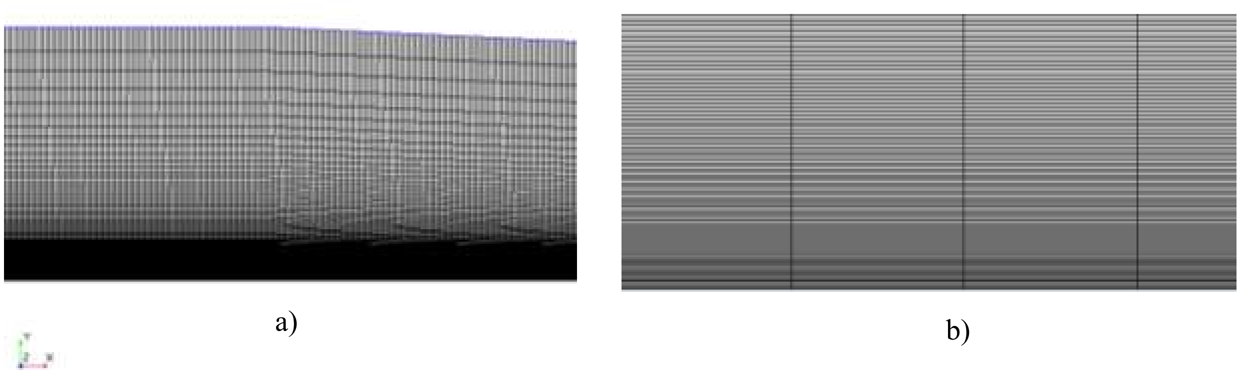

Fig. 3 a) Depiction of the mesh distribution, **b)** closeup of the near-wall region mesh.

The streamwise position x was normalized for each case using the corresponding inlet boundary layer thickness δ_{inlet} obtained by the corresponding simulation. The numerical results show a very good agreement with the analytical solution from the sink flow theory. This confirms that the computational domain and top inclined surface have been adequately designed. The theoretical analytical solution is given by the following equation:

$$\frac{U_\infty}{U_{\infty,i}} = \frac{1}{KU_\infty/v(x_i - x) + 1} \tag{12}$$

where U_∞ is the local free stream velocity, $U_{\infty,i}$ is the inlet free stream velocity, v is the kinematic viscosity, x_i is the inlet coordinate, x is the streamwise position, and K the acceleration parameter. It can be observed that, as the mesh was refined, the free stream velocities obtained by the RANS model actually deviated further from the analytical and DNS solution. However, maximum discrepancies were observed to be within 3%. The boundary layer thickness was calculated by performing a linear interpolation to find the y position at which the local streamwise velocity was 99% of the local free stream velocity.

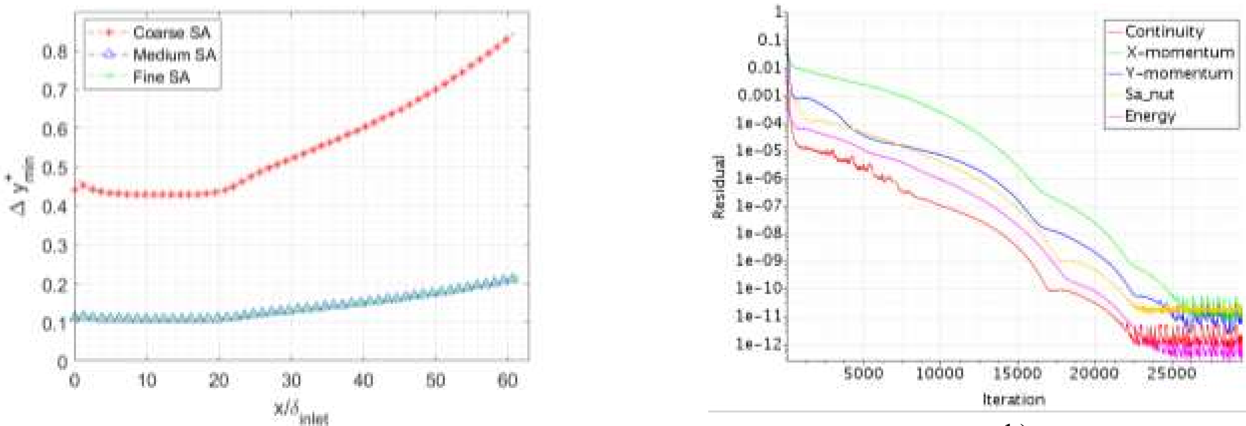

a) b)

Fig. 4 a) Near wall resolution and **b)** residual history of the fine mesh case.

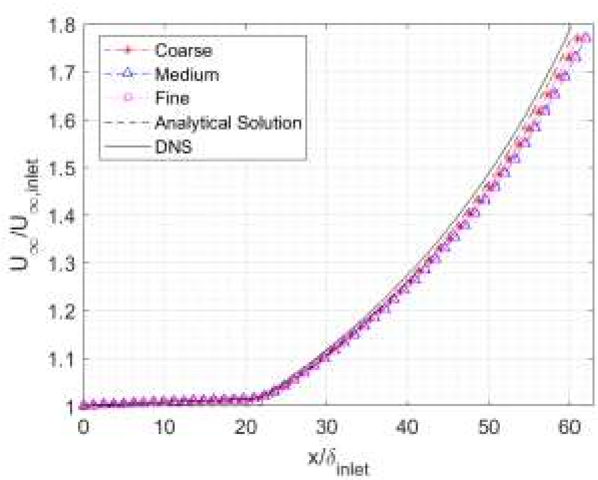

Fig. 5 Streamwise variation of the freestream velocity.

Spatial filtering of the boundary layer thickness in the x-direction is done by using a five-point averaging window, i.e. two points downstream and two points upstream at any given streamwise direction. Furthermore, boundary layer thicknesses were normalized by their respective inlet value. As the mesh was refined, the model increased its overprediction with a maximum error of approximately 6.5% (Fig. 6). Still, the SA turbulence model is able to capture fairly well the typical shrinking process of the boundary layer thickness in sink flows. The skin friction coefficient was calculated using the following formula:

$$C_f = \frac{\tau_w}{\frac{1}{2}\rho U_\infty^2} \tag{13}$$

where τ_w is the wall shear stress given by

$$\tau_w = \mu \frac{\partial \overline{U}}{\partial y}\bigg|_{wall} \tag{14}$$

where $\overline{U}$ is the mean streamwise velocity near the wall and y is the vertical distance from the wall. As the mesh was refined, the skin friction coefficient yielded lower values. An initial developing section can be observed in C_f profiles of Fig. 7 (and in the DNS data as well), this sudden increase may be caused by turbulence transition and triggering of turbulent events. The values then decrease in the ZPG zone (flat plate) and show a significant increase from the ZPG-FPG transition. The C_f profiles then show asymptotic trends towards approximately constant values by the end of the computational domain, which concur with

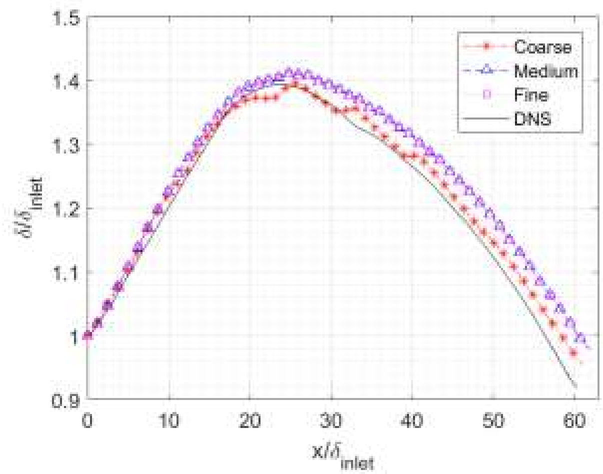

the sink flow theory [15].

Fig. 6 Streamwise variation of the velocity boundary layer.

However, the turbulence model does not seem capable of capturing the decrease of C_f which is a characteristic of the quasi-laminarization phenomenon [1] [10].

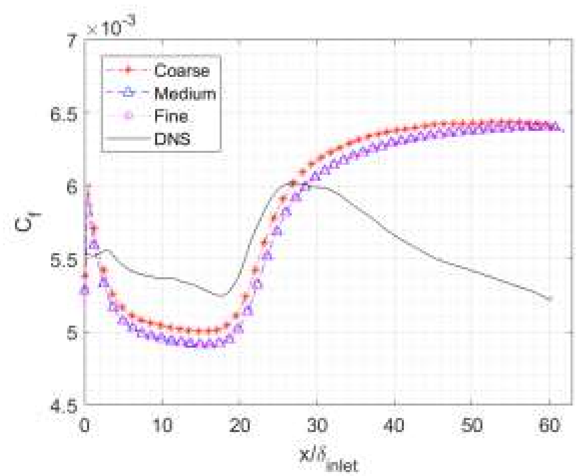

Fig. 7 Streamwise variation of the skin friction coefficient.

3.2 Assessment of Turbulence Models: Validation with DNS Data

The medium mesh was selected to perform the turbulence modeling comparison since refining it further presented no substantial difference in results. When predicting the free stream velocity, all three turbulence models showed very similar results with a maximum error percentage of 3% between the analytical solution and the SST model (Fig. 8). The models also show an increasing underprediction further downstream of the FPG zone. On the other hand, the DNS solution shows an approximately constant overprediction with a 1% of error.

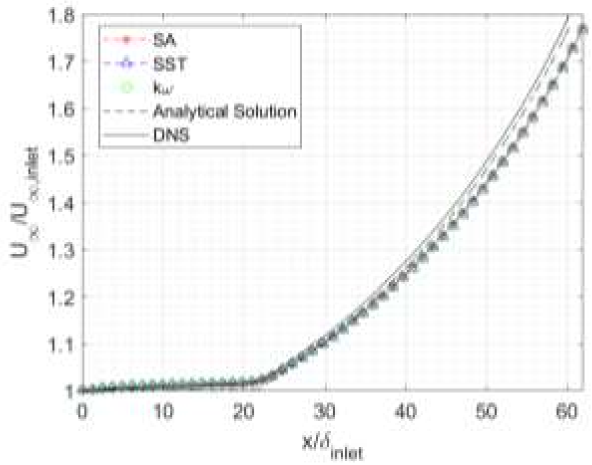

Fig. 8 Streamwise variation of the freestream velocity.

The acceleration parameter, *K*, was computed according to the following formula:

$$K = \frac{\upsilon}{U_\infty^2}\frac{dU_\infty}{dx} \tag{15}$$

where x is the streamwise location and υ is the kinematic viscosity. Streamwise smoothing was done using a five-point averaging window. The SST and k-ω models showed an "overshoot" or overprediction on K values near the inlet (Fig. 9). This could be attributed to the prescribed inlet conditions in the RANS simulations. Although we have imposed the streamwise and wall-normal components of the velocity as well as the temperature profiles from DNS, the turbulent viscosity ratio has been set constant and equal to 10. This approximation might be the reason of these inlet developing sections. Further studies will imply the inlet prescription of the turbulent viscosity ratio obtained from DNS, and will be published elsewhere. In the ZPG region, the theoretical values of the acceleration parameter should be zero (flat plate); however, some residual values in the order of 10^{-7} in DNS results reveal that the strong FPG causes an upstream influence with almost negligible values of K. SA predicts K very well in the ZPG region until $x/\delta_{inlet} \approx 9$. Then, the values for K show a steep increase as the flow accelerates. All three models underpredict K in the ZPG-FPG transition. The numerical K level off in the FPG zone from around $x/\delta_{inlet} \approx 30$ with excellent agreement with DNS results.

Figure 10a shows the skin friction coefficient along the streamwise direction. Results from two equation turbulence models, i.e. SST and k-ω, exhibit similar behaviors. In the ZPG zone, there is a significant underprediction of approximately 46% of discrepancies, which might be caused by incorrect inlet conditions particularly for the corresponding profiles of k (turbulent kinetic energy), ω and ε (dissipation). In the FPG zone, C_f profiles steadily increase, surpassing the DNS values and reaching a maximum error percentage of 31% for k-ω while 21% for SST. SA turbulence model gives a much better approximation of the skin friction coefficient in the ZPG zone with an initial overshoot and developing section, with maximum discrepancies in the order of 7% with respect to DNS. Furthermore, C_f from SA increases asymptotically in the FPG zone towards a maximum value of 6.2×10^{-3}, which is typical for a sink flow (e.g., constant values of the skin friction coefficient). However, since the imposed acceleration parameter K is larger than the critical value $K_{crit} = 3\times10^{-6}$, the skin friction coefficient is expected to decrease due to the quasi-laminarization process [1]. In fact, all three models fail to capture the decrease in friction coefficient caused by the quasi-laminarization effect. Boundary layer thickness was calculated and normalized as previously described. Again, similar values were obtained from the k-ω and SST models. Both models show considerable deficiencies in modeling the boundary layer thickness with errors reaching approximately 25%. In contrast, SA's results are very similar to those obtained by the DNS model. The SA model appropriately capture the shrinking process of the boundary layer in highly accelerated flows. The largest difference occurs in the FPG zone where the model overpredicts the boundary layer thickness by 8%.The friction velocity was calculated as follows:

$$U_\tau = \sqrt{\frac{\tau_w}{\rho}} \tag{16}$$

The friction velocity obtained with the k-ω and SST data was found to show an underprediction in the ZPG zone with a fast decrease and slow increase (Fig. 11) whereas the values of U_τ from SA remain nearly constant (as expected in a canonical boundary layer or flat plate flow) but still some slight underpredictions with respect to DNS data can be observed. As the flow accelerates in the FPG zone, the values from all models increase, as expected, until they exceed the ones from the DNS. This confirms the insensitiveness of turbulence models to capture the effects of quasi-laminarization.

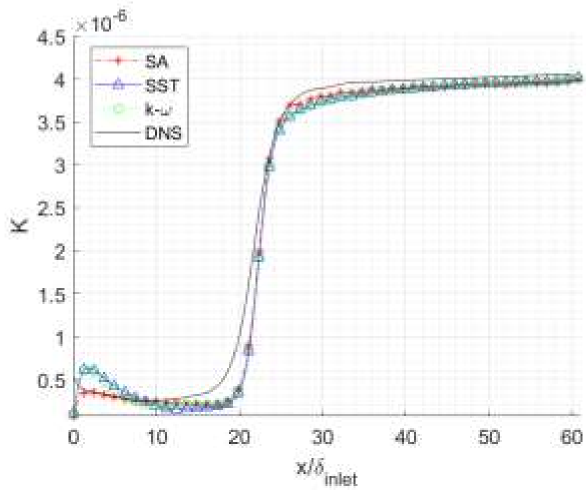

Fig. 9 Streamwise variation of the acceleration parameter.

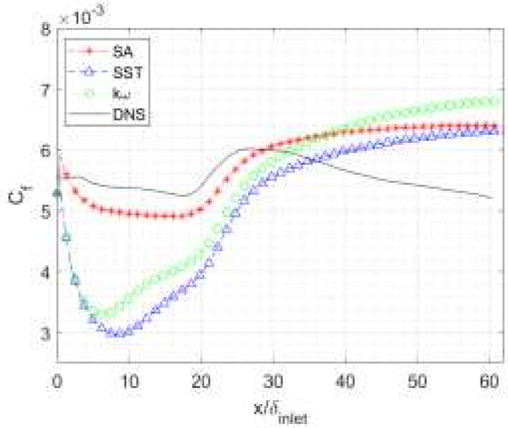

a)

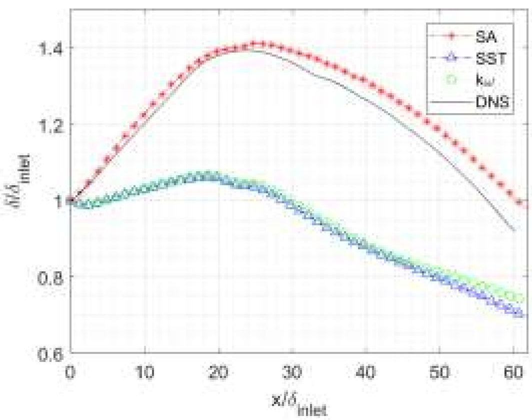

b)

Fig. 10 Streamwise variation of (a) the friction coefficient and (b) the boundary layer thickness.

The momentum thickness Reynolds number was calculated using:

$$Re_\theta = \frac{U_\infty \theta}{\upsilon} \tag{17}$$

where θ is the momentum thickness. The momentum thickness was computed in MATLAB using the discretized form of the following formula:

$$\theta = \int_0^\infty \frac{U}{U_\infty}\left(1 - \frac{U}{U_\infty}\right) dy \tag{18}$$

where U is the local streamwise velocity.

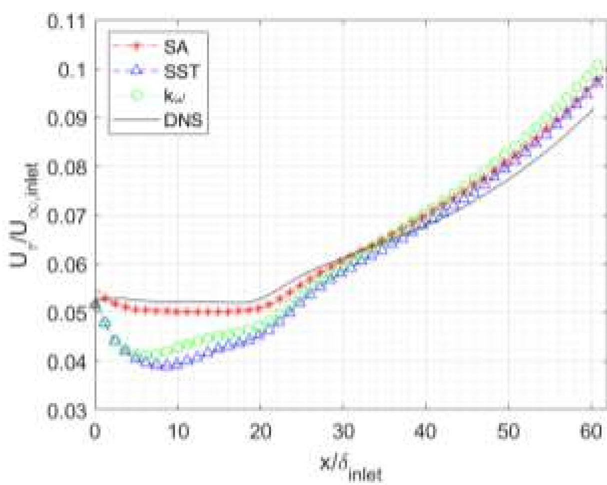

Fig. 11 Streamwise variation of the friction velocity.

The momentum thickness Reynolds number computed from the results of SST and *k-ω* models were significantly lower than the ones obtained from DNS (Fig. 12). However, they show the expected linear increase in the ZPG or canonical boundary layer. The results from the SA data yield higher momentum thickness Reynolds numbers with a significantly better agreement with DNS. They also show a linear increase until the ZPG-FPG transition where it levels off. The Re_θ profiles from RANS models show an evident decreasing tendency in the FPG zone, which may indicate that turbulence models are capturing the quasi-laminarization stage. However, it can be seen that Re_θ profiles from turbulence models tend towards a 'plateau'. Moreover, another characteristic of sink flows, which are not laminarizing, is to exhibit constant values of Re_θ [1].

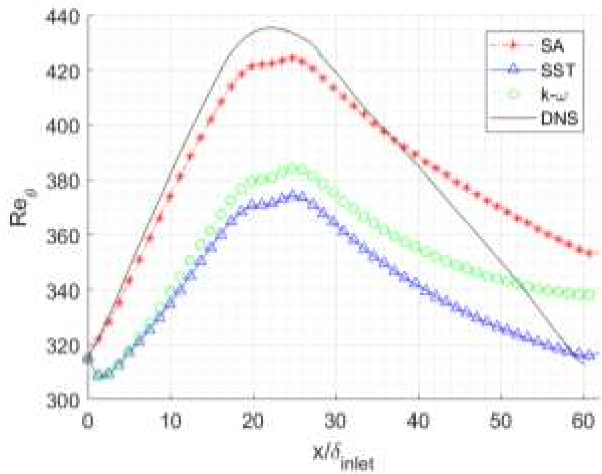

Fig. 12 Streamwise variation of the momentum thickness Reynolds number.

The nondimensional wall distance, y^+, was calculated by multiplying the wall distance, y, by the friction velocity and dividing it by the kinematic viscosity. The time-averaged streamwise velocity was also normalized in inner units by dividing it by the friction velocity. These velocity profiles were graphed at four streamwise locations in terms of the inlet boundary layer thickness, i.e., x/δ_{inlet} = 10, 30, 40 and 55, respectively, as seen in Fig. 13. The good performance of the SA model in canonical boundary layers is evident according to Fig. 13a, which depicts an excellent agreement with DNS results up to the log region, and mild discrepancies are observed in the wake region and above. The significant discrepancies in u^+ profiles obtained by the two-equation models are mainly caused by the underprediction of the friction velocity in the ZPG zone. As the flow penetrates into the strong FPG region, the effect of quasi-laminarization on u^+ profiles by DNS can be identified as a thickening of the viscous layer. In other words, the u^+ profiles move closer to the linear trend $u^+ = y^+$. Furthermore, the velocity profiles shift upwards the log region, showing obvious 'overshoots' and tending towards the Blasius solution [10] (not shown here). Moreover, the wake region nearly disappears by the end of the computational domain. Generally speaking, all turbulence models fail to accurately predict the time-averaged streamwise velocity in the FPG region in the buffer region ($y^+ > 10$) and above, inside the boundary layer. Since the turbulence models are always in 'on' mode, there is an overprediction of the turbulent eddy viscosity, and, consequently of the Reynolds shear stresses (turbulent mixing). A potential improvement over these turbulence models could be designed by limiting the turbulence production of highly accelerated flows based on the measured local K parameter. However, further investigation need to be performed in this line of research.

Figure 14 depicts the streamwise variation of the thermal boundary layer thickness δ_T. Once again, the SA model has demonstrated a superior performance with respect to two-equation models. The increasing linear trend of δ_T for ZPG flows is also captured by SA, showing an excellent agreement with DNS data. Downstream, the SA model is able to reproduce the thermal boundary layer shrinking in sink flows with maximum discrepancies in the order of 7%. Since the decrease of δ_T is not as aggressive as in δ, we may infer that the effect of strong FPG is mainly manifested in the velocity field. In other words, while pressure may directly affect the velocity field in incompressible flows, the thermal field is indirectly influenced by pressure only through velocity.

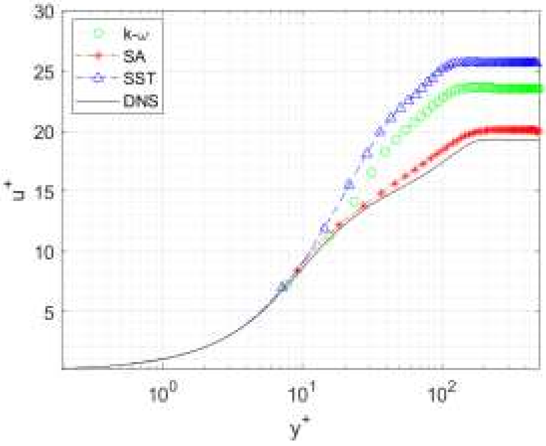

a)

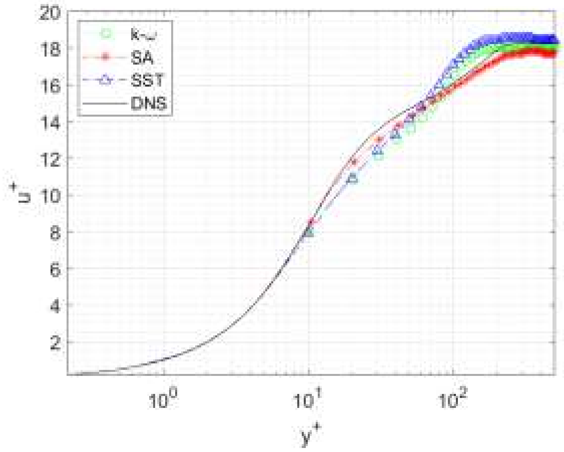

b)

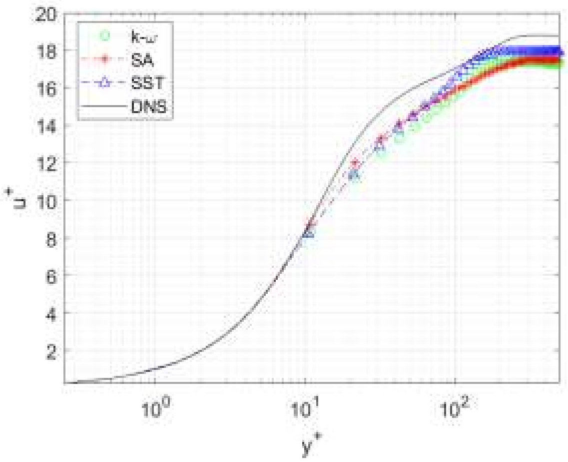

c)

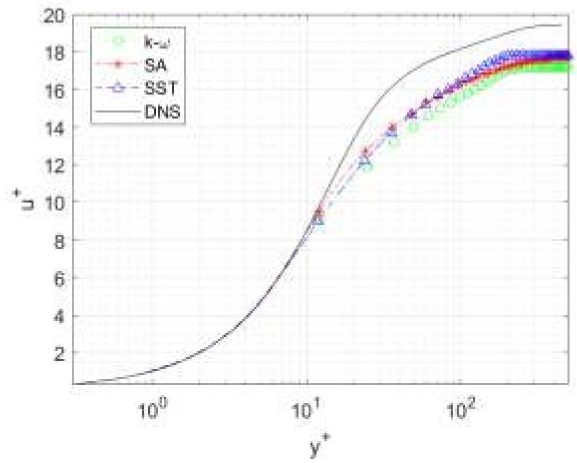

d)

Fig. 13 Profiles of mean streamwise velocity in wall units at **a)** $x/\delta_{inlet} = 10$, **b)** $x/\delta_{inlet} = 30$, **c)** $x/\delta_{inlet} = 40$, and **d)** $x/\delta_{inlet} = 55$.

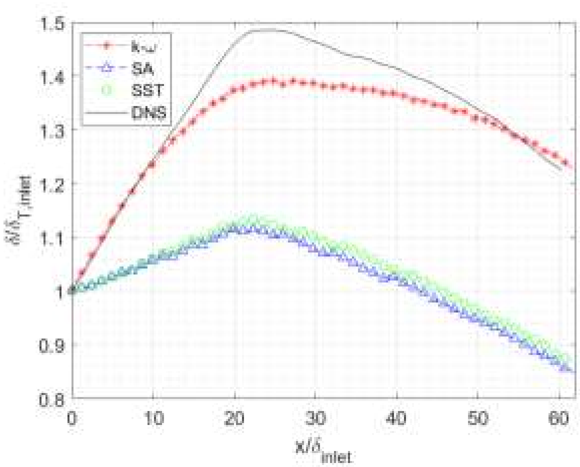

Fig. 14 Streamwise variation of the thermal boundary layer thickness.

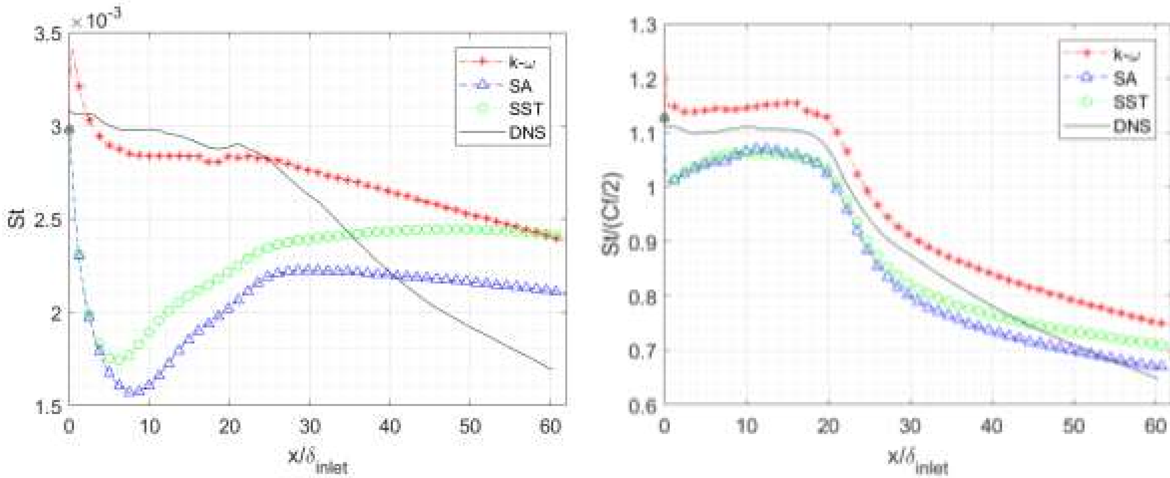

a) b)

Fig. 15 Streamwise variation of (a) Stanton number and (b) Reynolds analogy.

The Stanton number is defined as:

$$St = \frac{|q_w|}{\rho C_p U_\infty (T_\infty - T_w)} \tag{19}$$

where the wall heat flux is,

$$q_w = -k \left.\frac{\partial T}{\partial y}\right|_w \tag{20}$$

Figure 15 a) shows the streamwise development of the Stanton number. Results from RANS exhibit a lengthy developing section (triggering of turbulence), which is more pronounced in two-equation models. In DNS, the sharp decrease of *St* in the FPG zone is mainly caused by flow acceleration (i.e., increase of U_∞) since the wall heat flux has been observed to slightly decrease. Only the SA model has been able to somehow reproduce the decreasing trend of *St* en the FPG zone. The Reynolds analogy ratio $St/(C_f/2)$ is shown in figure 15 b). In the ZPG zone, DNS gives almost constant values above one, since the Prandtl number is lower than the unitary value (i.e., Pr = 0.71). Interestingly, all turbulence models show a fair agrement with DNS results in the FPG zone. This may be attributed to some error compensation in C_f and *St* computation from RANS. The low values of the ratio $St/(C_f/2)$ beyond $x/\delta_{inlet} = 30$ reveals a breakdown of the Reynolds analogy in higly accelerated flows.

Figure 16 depicts the time-averaged temperature at four streamwise stations and normalized in inner units by the friction temperature $\theta_\tau = \mathrm{St}(T_\infty - T_w)U_\infty/u_\tau$. Major conclusions are three-fold: (i) FPG effects on thermal profiles are not as obvious as in velocity profiles, a log region is still observed at $y^+ \approx 100$ in the streamwise location of $x/\delta_{inlet} = 30$, (ii) a very good performance of the SA model is seen up to $x/\delta_{inlet} \approx 30$, and (iii) the 'overshoot' on the thermal profile of DNS in the buffer layer ($20 < y^+ < 50$) by the end of the computation domain (i.e., $x/\delta_{inlet} \approx 55$) indicates the presence of the quasi-laminarization process, which is not captured by any of the turbulence models. In the 'overshoot' zone of temperature profiles, local increases of the thermal gradient reveal augmentation of heat transfer by conduction, while thermal mixing due to wall-normal turbulent heat fluxes is attenuated by quasi-laminarization.

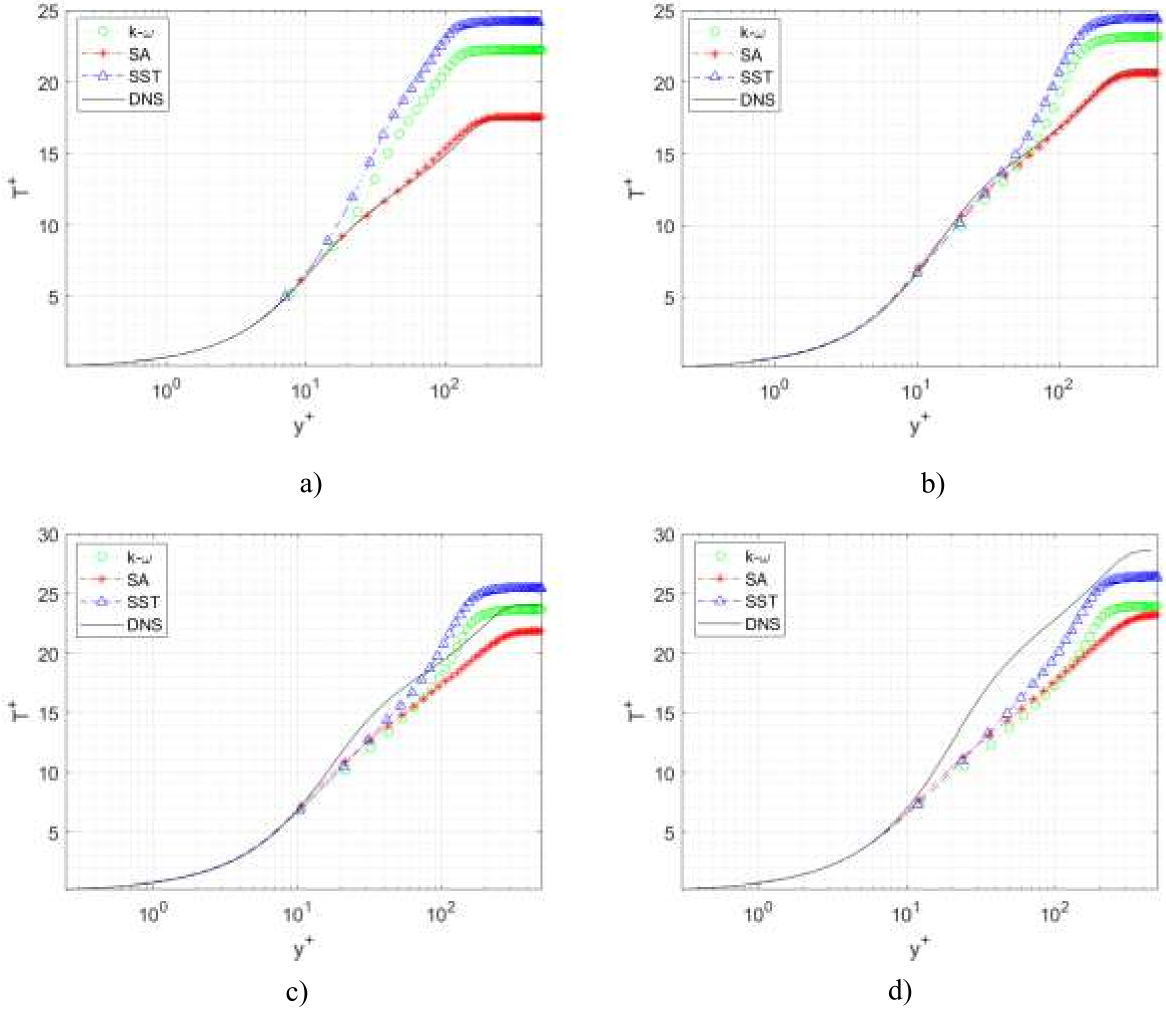

Fig. 16 Profiles of mean temperature in wall units at **a)** $x/\delta_{inlet} = 10$, **b)** $x/\delta_{inlet} = 30$, **c)** $x/\delta_{inlet} = 40$, and **d)** $x/\delta_{inlet} = 55$.

4. FINAL REMARKS

A numerical analysis is performed in sink-flow boundary layers subject to very strong FPG for the velocity and passive scalar field. In the RANS approach, three different turbulence models are considered: the Shear Stress Transport model (SST) by Menter, the *k-ω* model by Wilcox and the Spallart-Allmaras model. Validation against DNS data has been performed by reproducing the geometry aspects and boundary conditions as in Araya *et al*. (2015). The major conclusions are summarized as follows: (i) generally speaking, the SA model has demonstrated to be superior to the SST and *k-ω* models for the tested configuration, (ii) all turbulence models have significantly fallen to capture the quasi-laminarization process, and (iii) the velocity field is observed to be more susceptible to very strong FPG than the thermal field.

ACKNOWLEDGMENT

GS acknowledges the 2018-2019 NASA PR Space Grant Fellowship (Grant #NNX15AI11H). GA acknowledges AFOSR grant FA9550-17-1-0051 and NSF-GECAT grant #1440733. Computational resources were supplied by XSEDE (project #TG-CTS170006).

NOMENCLATURE

K	acceleration parameter	(-)
θ	momentum thickness	(m)
Re_θ	momentum thickness Reynolds number	(-)
y^+	wall distance in inner units	(-)
U^+	streamwise velocity in inner units	(-)

REFERENCES

[1] Sreenivasan, K.R., "Laminarescent, relaminarizing and retransitional flows", *Acta Mechanica,* 44, pp. 1–48, (1982).
[2] Jones, W.P., Launder, B.E., "Some properties of sink-flow turbulent boundary layers", *J. Fluid Mech.,* 56, pp. 337–351, (1972).
[3] Jones, M.B., Marusic, I., Perry, A.E., "Evolution and structure of sink-flow turbulent boundary layers", *J. Fluid Mech.*, 428, pp. 1–27, (2001).
[4] Perry, A.E., Henbest, S.M., Chong, M.S., "A theoretical and experimental study of wall turbulence", *J. Fluid Mech.,* 165, pp. 163–199, (1986).
[5] Narasimha, R., "Relaminarization – magnetohydrodynamic and otherwise", *In AIAA Progress in Astronautics and Aeronautics*, vol. 84, pp. 30–52, (1983).
[6] Narasimha, R., Sreenivasan, K.R., "Relaminarization of fluid flows", *Adv. Appl. Mech.,* 19, pp. 221–309, (1979).
[7] Schraub, A., Kline, S.J., "A study of the structure of the turbulent boundary layer with and without longitudinal pressure gradients", Report MD-12, Thermosciences Division, Mechanical Engineering Department, University of Stanford, (1965).
[8] Sreenivasan, K.R., "Laminarescent, relaminarizing and retransitional flows", *Acta Mechanica,* 44, pp. 1–48, (1982).
[9] Dixit, S.A., Ramesh, O.N., "Large-scale structures in turbulent and reverse-transitional sink flow boundary layers", *J. Fluid Mech.,* 649, pp. 233–273, (2010).
[10] Araya, G., Castillo, L., Hussain, F., "The log behaviour of the Reynolds shear stress in accelerating turbulent boundary layers", *J. Fluid Mech.*, 775, pp. 189-200, (2015).
[11] Araya, G., Rodriguez, D., "Visualization and assessment of turbulent coherent structures in laminarescent boundary layers", *J. Vis.*, 21, pp. 191-202, (2018).
[12] Araya, G., Jansen, K., Meneveau, C., Castillo, L., "A dynamic multi-scale approach for turbulent inflow boundary conditions in spatially evolving flows", *J. Fluid Mech.*, 670, pp. 518–605, (2011).
[13] Lund, T.S., Wu, X., Squires, K. D., "Generation of turbulent inflow data for spatially developing boundary layer simulations", *J. Comput. Phys.*, 140, pp. 233–258, (1998).
[14] *STAR-CCM+® Documentation: Version 13.02,* (2018).
[15] Rosenhead, L., "Laminar Boundary Layers", *Oxford University Press*, (1963).